

# TeV-peaked candidate BL Lac objects

L. Costamante<sup>1</sup>

<sup>1</sup>ASI – Unità Ricerca Scientifica, Via del Politecnico snc, I-00133, Roma, Italy

Accepted 2019 October 23. Received 2019 October 23; in original form 2019 August 23.

## ABSTRACT

BL Lac objects can be extreme in two ways: with their synchrotron emission, peaking beyond 1 keV in their spectral energy distribution, or with their gamma-ray emission, peaking at multi-TeV energies up to and beyond 10-20 TeV, like 1ES 0229+200. This second type of *extreme BL Lacs* – which we can name *TeV-peaked BL Lacs* – is not well explained by the usual synchrotron self-Compton scenarios for BL Lacs. These sources are also important as probes for the intergalactic diffuse infrared background and cosmic magnetic fields, as well as possible sites of production of ultra-high-energy cosmic rays and neutrinos. However, all these studies are hindered by their still very limited number. Here I propose a new, simple criterium to select the best candidates for TeV observations, specifically aimed at this peculiar type of BL Lac objects by combining X-ray, gamma-ray and infrared data. It is based on the observation of a clustering towards a high X-ray to GeV gamma-ray flux ratio, and it does not rely on the radio flux or X-ray spectrum. This makes it suitable to find TeV-peaked sources also with very faint radio emission. Taking advantage of the *Fermi* all-sky gamma-ray survey applied to the ROMA-BZCAT and Sedentary Survey samples, I produce an initial list of 47 TeV-peaked candidates for observations with present and future air-Cherenkov telescopes.

**Key words:** BL Lacertae objects: general – Gamma rays: galaxies

## 1 INTRODUCTION

BL Lac objects are a particular type of blazars, namely radio-loud active galactic nuclei (AGN) with the relativistic jet pointing towards us. They are the most copious emitters of very high energy radiation (VHE,  $\gtrsim 0.1$  TeV, e.g. Aharonian et al. 2008a) in the extragalactic sky, especially after accounting for the absorption effect due to  $\gamma$ - $\gamma$  interactions with the diffuse Extragalactic Background Light (EBL, see e.g. Hauser & Dwek 2001; Domínguez et al. 2011; Franceschini & Rodighiero 2017, and references therein). Their spectral energy distribution (SED) is dominated by non-thermal radiation, and is characterized by two distinctive broad humps, peaking at low and high energy, commonly (but not uniquely) explained as synchrotron and inverse Compton (IC) emission from a population of relativistic electrons in the jet.

BL Lac objects span a wide range of synchrotron peak frequencies, from infrared (IR) to X-ray energies, justifying the division in “Low-” and “High-frequency peaked” BL Lacs (LBL and HBL, respectively, Padovani & Giommi 1995), or the more recent “Low-”, “Intermediate-” and “High-Synchrotron Peaked” sources (LSP, ISP and HSP, Abdo et al. 2010). Correspondingly, their high-energy peak in gamma-rays shifts from MeV up to TeV energies. This sequence of SEDs seems anti-correlated with the bolometric luminosity of the objects, forming the main part of the so-called “blazar sequence” (Ghisellini et al. 2017). Compton dominance plays a crucial role since its inception (see Fossati et al. 1998; Finke 2013). However, it is still debated if this correlation has an underlying physical origin or it is just the result of selection

biases, given that a significant fraction of the BL Lac population is still missing redshift measurements (see e.g. Giommi et al. 2012, for an alternative view).

Extreme BL Lacs populate the highest-energy end of the blazar sequence. They come in two varieties, according to whether the extreme properties are shown in the low (synchrotron) or high energy emission.

The ‘BL Lacs extreme in synchrotron’ are characterized by hard<sup>1</sup> synchrotron X-ray spectra ( $\alpha_x < 1$ ) at least up to  $\sim 1$  keV, locating the synchrotron peak energy above 1 keV, an order of magnitude higher than regular HBL. In these objects the peak energy can reach 100 keV and beyond, as in 1ES 1426+428. These objects are called “Extreme synchrotron BL Lacs” (Costamante et al. 2001) or “Extreme HSP” (EHSP, Arsioli et al. 2018). Some authors define EHSP the objects with  $\nu_{peak} > 10^{17}$  Hz (corresponding to 0.4 keV), but here we will adopt the original stricter definition of  $> 1$  keV, which has the advantage of a more direct assessment through the shape of the X-ray spectrum instead of a model of the SED.

The ‘BL Lacs extreme in gamma-rays’ are instead characterized by hard intrinsic VHE spectra ( $\alpha_{VHE} < 1$ ) up to and beyond  $\sim 1$  TeV, after correction for the EBL absorption effects. This occurs in some sources even considering the lowest possible EBL given by galaxy counts (e.g. Aharonian et al. 2006, 2007c),

<sup>1</sup> Spectra are called hard or soft if the power-law spectral index  $\alpha < 1$  or  $\alpha > 1$  respectively (i.e. photon index  $\Gamma < 2$  or  $\Gamma > 2$ ). This convention corresponds to spectra rising or decaying with frequency in the SED.

locating their gamma-ray peak assuredly above 1 TeV, an order of magnitude higher than in regular HBL. These sources are called “*extreme-TeV BL Lacs*” (Tavecchio et al. 2011) or “*hard-TeV BL Lacs*” (Costamante et al. 2018), and have been introduced as a new class of BL Lac objects in Bonnoli et al. (2015). They are also generically referred to as “*extreme HBL*” (EHBL) although the two measures of extremeness –in synchrotron and gamma-rays– do not always go together (see e.g. Costamante et al. 2018; Foffano et al. 2019). The prototype of this class is 1ES 0229+200, which is the most extreme case discovered so far with a hard VHE spectrum of  $\alpha_{\text{VHE}} \sim 0.5$  and a gamma-ray peak well beyond 10 TeV.

While a synchrotron peak of even 100 keV or more represents no problem in standard shock-acceleration scenarios, being well below the maximum frequency that can be produced by electrons accelerated at the maximum possible rate ( $h\nu_{\text{peak}}/\delta \sim 1\text{--}10$  KeV  $\ll$  150 MeV,  $\delta$  being the beaming factor; see e.g. Aharonian 2004), a gamma-ray peak at multi-TeV energies is difficult to obtain by IC in blazars, for standard one-zone leptonic models of the SED. Both the decrease of the scattering efficiency in the Klein-Nishina regime and the lower energy density of the seed photons available for scatterings in the Thomson regime, as the gamma-ray energy increases, tend to steepen the TeV spectrum. A synchrotron self-Compton (SSC) mechanism can still work, but at the price of a narrow electron distribution which does not reproduce the SED at UV and lower frequencies with a single population of electrons. Furthermore, it requires extremely high electron energies, very low radiative efficiency and conditions strongly out of equipartition by several orders of magnitude (Costamante et al. 2018). Radically different alternative scenarios have been proposed, from internal  $\gamma$ - $\gamma$  absorption on a Planckian radiation field (Aharonian et al. 2008b) to a separate origin for the X-ray and TeV emissions, the latter coming from kpc-scale jets (Böttcher et al. 2008) or secondary emission from cascades (e.g. Essey et al. 2011; Prosekin et al. 2012).

These extreme-TeV BL Lacs represent today a major challenge for the known acceleration and emission processes in blazar’s jets. In addition, they are of great interest as probes of the near-infrared part of the diffuse EBL (e.g. Costamante 2013; Franceschini & Rodighiero 2017) and cosmic magnetic fields (e.g. Dolag et al. 2009; Neronov & Vovk 2010; Finke et al. 2015), as well as possible sources of ultra-high-energy cosmic rays and neutrinos (e.g. Padovani et al. 2016; Resconi et al. 2017).

However, their number is still limited to a handful, essentially because of the lack of systematic searches and of an all-sky survey at VHE with sufficient sensitivity. To identify more sources of this type among generic BL Lacs, the measurement of the VHE spectrum is mandatory, since it is the only way to determine the hardness or softness of their VHE emission and with it the location of the gamma-ray peak. Sufficient photon statistics is also required to constrain the gamma-ray peak in a meaningful way. At present this is best achieved with imaging air Cherenkov telescopes arrays, which however have the disadvantage of a narrow field of view and limited duty cycle, requiring dedicated campaigns.

The purpose of this paper is to introduce a simple and handy criterium to select the most promising TeV-peaked candidates for pointed observations with present and future air-Cherenkov telescopes. This is different from our previous work (Costamante & Ghisellini 2002) and from most of the recent selections (e.g. Tavecchio et al. 2010; Massaro et al. 2013; Bonnoli et al. 2015; Chang et al. 2017; Arsioli et al. 2018). The focus here is not on finding merely TeV-emitting sources, either normal or extreme synchrotron, but rather *TeV-peaked* sources, namely those TeV-

**Table 1.** Established Hard-TeV BL Lacs, as of December 2018. The intrinsic photon index  $\Gamma_{\text{intr.}}$  is the index of the power-law fit of the VHE spectrum corrected for EBL absorption according to Domínguez et al. (2011), over the reported energy band. The last column gives the references for the VHE data: 1) Aharonian et al. (2007c); 2) Aliu et al. (2014); 3) Aharonian et al. (2007b); 4) Abramowski et al. (2012); 5) Aharonian et al. (2010); 6) Acciari et al. (2010); 7) Aharonian et al. (2007a); 8) Aharonian et al. (2006); 9) Madhavan (2013); 10) Acciari et al. (2009); 11) Abramowski et al. (2010); 12) Costamante (2012).

Name	$z$	$\Gamma_{\text{intr.}}$	Energy TeV	refs
1ES 0229+200	0.140	$1.5 \pm 0.2$	0.6–12	1,2
1ES 0347–121	0.188	$1.8 \pm 0.2$	0.25–3	3
1ES 0414+009	0.287	$1.9 \pm 0.3$	0.15–2	4
PKS 0548–322	0.069	$2.0 \pm 0.3$	0.3–4	5
RGB J0710+591	0.125	$1.8 \pm 0.2$	0.3–4	6
1ES 1101–232	0.186	$1.7 \pm 0.2$	0.2–4	7,8
1ES 1218+304	0.182	$1.9 \pm 0.1$	0.2–4	9,10
H 2356–309	0.165	$1.95 \pm 0.2$	0.2–2	11,12

emitting BL Lacs with hard TeV spectrum and the gamma-ray peak above 1 TeV.

In the following, we refer to these objects equivalently as TeV-peaked BL Lacs or hard-TeV BL Lacs, depending on whether the emphasis is on the physical SED properties or on the direct observational feature. Unless otherwise stated, a flat  $\Lambda$ CDM cosmology is used with  $h = \Omega_{\Lambda} = 0.7$ . The VHE spectra are corrected for EBL absorption effects using the calculations by Domínguez et al. (2011). Spectral indices  $\alpha$  are defined by flux density  $S_{\nu} \propto \nu^{-\alpha}$  and correspondingly photon indices  $\Gamma \equiv \alpha + 1$  are defined by number density  $N(E) \propto E^{-\Gamma}$ .

## 2 HARD-TEV VS SOFT-TEV BLLACS

According to the online catalog of TeV-detected sources (TeV-Cat<sup>2</sup>), as of December 2018 there are 49 HBL detected at VHE. Out of these, 12 objects have no or uncertain redshift, and 4 objects do not have a published VHE spectrum yet. It is thus not possible to derive their intrinsic EBL-corrected spectrum. Of the remaining 33 HBL, 22 have soft TeV spectra while 8 show hard TeV spectra (namely with nominal  $\Gamma_{\text{intr}} \leq 2$ ), though two might be considered borderline or transitional, given the error on their slope and the almost flat spectrum (namely PKS 0548-322 and H 2356-309). The hard sources are listed in Table 1, along with their EBL-corrected spectral slope.

Based on this limited sample, hard-TeV BL Lacs seem to constitute about 1/4 of all detected HBL so far, not considering for the moment 3 objects which have shown both hard and soft spectra in different datasets, namely Mkn 501 (Aharonian et al. 1999; Ahnen et al. 2018), 1ES 1727+502 (Aleksić et al. 2014; Archambault et al. 2015) and 1ES 1741+196 (Abeysekara et al. 2016; Ahnen et al. 2017). These demonstrate however that a hard TeV spectrum is not always a permanent property, and that HBL can undergo strong shift of the SED peak towards high energies in the gamma-ray band as well as in the X-ray band.

At high energies (HE, 0.1–100 GeV), the band where the *Fermi* Large Area Telescope (LAT,  $\sim 0.1$ –800 GeV, Atwood et al. 2009)

<sup>2</sup> <http://tevcat.uchicago.edu/>

is most sensitive, all HBL display a hard spectrum (i.e.  $\alpha_\gamma \lesssim 1$ ), because the LAT is sampling the emission longward of the gamma-ray peak. However, hard-TeV BL Lacs have generally a much lower flux in *Fermi* than soft-TeV objects, at similar SED luminosities. As the gamma-ray peak shifts towards multi-TeV energies, the LAT band falls more and more inside the valley between synchrotron and Compton humps, where the emission is much weaker. Regular soft-TeV HBL peak around 30–300 GeV, and therefore tend to be much brighter in *Fermi* for the same bolometric luminosity, because the peak is closer to the LAT passband. Indeed, this was the case during the first years of *Fermi* operation: among the known TeV BL Lacs, the first ones detected by *Fermi*-LAT were always characterized by soft intrinsic VHE spectra (e.g. [Abdo et al. 2009](#)). As for any telescope, *Fermi*-LAT tends to detect sources with the peak emission in or close to its passband, and for HBL this means a bias for the soft-TeV type.

To find new hard-TeV sources, therefore, somewhat counter-intuitively we need to look for objects with the *lowest* –not the highest– gamma-ray flux in *Fermi*-LAT, for a given synchrotron flux. The latter can be traced by the X-ray flux around 1 keV, which is close to the peak of the synchrotron emission in HBL. The most promising TeV-peaked candidates, therefore, should be those with the largest X-ray to GeV flux ratio, i.e. with the highest broad-band index  $\alpha_{x\gamma}$ . In the following sections, this criterium is applied to a large sample of BL Lacs, and further refined with information from the Wide-field Infrared Survey Explorer (WISE).

### 3 THE SAMPLE AND BROAD BAND INDICES

The sample of BL Lac objects considered here is constructed by merging the 5BZCAT blazar collection ([Massaro et al. 2015](#)) with the “Sedentary Survey” sample, which selects by construction extreme HBL ([Giommi et al. 2005](#)). Only established BL Lac objects with both X-ray and radio data are considered, for a total number of 1170 objects of every SED type. Nearly all of the 150 BLLacs in the Sedentary sample are comprised in the 5BZCAT, with the exception of three: SHBL J101616.7+410812, SHBL J142739.5-252102 and SHBL J224340.1-123100 (the latter detected by *Fermi*-LAT as 3FGL J2243.6-1230). This total sample is then feeded with additional data taken from the gamma-ray (*Fermi*-LAT) and infrared (WISE) source catalogs.

The 1-100 GeV gamma-ray fluxes and photon indices are obtained from the Third *Fermi*-LAT AGN catalog (3LAC, [Ackermann et al. 2015](#)). For the objects not detected in the 3LAC, a reference flux of  $8 \times 10^{-11} \text{ cm}^{-2} \text{ s}^{-1}$  is adopted, with a photon index  $\Gamma \equiv 1.7$  (appropriate for HBL, midway between the average index of the hard-TeV objects,  $\sim 1.6$ , and soft-TeV ones,  $\sim 1.8$ ). This flux corresponds to a level just below the lowest flux detected in the 3LAC catalog ( $8.7 \times 10^{-11}$ ), and should be considered as an upper limit.

The 0.1–2.4 keV X-ray fluxes are taken from the values listed in the catalogs with the following order of priority: 3LAC, Sedentary Survey, 5BZCAT. Because the X-ray flux reported in the 5BZCAT is not corrected for galactic absorption, unlike the 3LAC and Sedentary Survey values, a multiplication factor is introduced to approximately compensate for the absorbed flux, as follows:  $1.7 \times$  if the galactic column density  $N_{\text{H}}$  is  $< 5 \times 10^{20} \text{ cm}^{-2}$ ,  $2.0 \times$  if it is between 5 and  $10 \times 10^{20}$ , and  $3.0 \times$  if  $\geq 10^{21} \text{ cm}^{-2}$ . These values are derived from tests in XSPEC with photon indices in the range 1.5-2.3. The galactic average  $N_{\text{H}}$  is derived from the `nh` tool with the values from LAB survey maps ([Kalberla et al. 2005](#)).

Monochromatic fluxes at 1 keV and 1 GeV are then calculated from integrated fluxes assuming a power-law spectrum, using the spectral indices from the respective catalogs. For the X-ray spectral index, a value of  $\alpha_{\text{X}} = 1.1$  is used, as in the Sedentary Survey, unless the gamma-ray photon index is  $\Gamma > 2.2$ . In that case,  $\alpha_{\text{X}} = 0.8$  is adopted, to better approximate the slope of the X-ray emission in objects with LSP-type SED (which are characterized by steep GeV spectra).

The infrared data are taken from the ALLWISE Source Catalog as provided by the NASA/IPAC Infrared Science Archive (IRSA), with a cross-matching radius of  $3.5''$ . The magnitude  $m_3$  in the W3 filter measured with profile-fitting photometry (`w3mpfro`) is converted to flux density at the effective frequency  $\nu_{\text{iso}} = 2.6753 \times 10^{13} \text{ Hz}$  with the formula  $F_{\text{W3}}(mJy) = 31674 \times 10^{-m_3/2.5}$  ([Jarrett et al. 2011](#)). The infrared spectral index is calculated from the fluxes in the W3 and W2 filters.

The broad-band indices  $\alpha_{x\gamma}$  and  $\alpha_{\text{wx}}$  between the X-ray (1 keV), gamma-ray (1 GeV) and infrared (W3) frequencies are then computed from the monochromatic fluxes according to the following formula:

$$\alpha_{12} \equiv - \frac{\log \left( \frac{F_1}{F_2} * k \right)}{\log \left( \frac{\nu_1}{\nu_2} \right)} \quad (1)$$

where  $F_n$  is the flux at the frequency  $\nu_n$  and  $k = (1+z)^{\alpha_2 - \alpha_1}$  is the total K-correction factor, with  $\alpha_1$  and  $\alpha_2$  being the spectral indices at the respective frequencies. The broad-band index is essentially the ratio of the monochromatic fluxes at two different energies, and represents the spectral index of a power-law spectrum connecting the two flux points ([Stocke et al. 1991](#); [Padovani & Giommi 1995](#)). For the K-correction when the redshift is unknown, a value of  $z = 0.3$  is assumed, which is the average redshift of HSP blazars in the 3LAC and Sedentary Survey samples.

### 4 TEV-PEAKED CANDIDATES SELECTION

Figure 1 shows  $\alpha_{x\gamma}$  as a function of the X-ray flux, for all BL Lacs in the total sample. Indeed *the known hard-TeV BL Lacs cluster in the region of high  $\alpha_{x\gamma}$  and high X-ray flux*. We can interpret this property as follows: the index  $\alpha_{x\gamma}$  works as a proxy for the location of the gamma-ray peak (namely, it tells how deep the LAT flux is inside the valley between the two SED humps), while the X-ray flux works as a proxy for the synchrotron peak luminosity, in itself a tracer of the number of high-energy electrons in the source. It thus gives an estimate of the “flux caliber” of the source for the detectability by Cherenkov telescopes.

Assuming a Compton dominance close to one (i.e.  $L_{\text{IC}} \sim L_{\text{synch}}$ ), sources with the higher  $\alpha_{x\gamma}$  and X-ray flux are more likely to have a gamma-ray peak at TeV energies and with higher flux. The region of high  $\alpha_{x\gamma}$  and high X-ray flux determined by the location of the known TeV-peaked objects can thus be considered a good criterium for the selection of new TeV-peaked candidates. To do so, a selection region is drawn at  $\alpha_{x\gamma} > 1.15$  and  $\text{Log}(\nu_{\text{x}} F_{\text{x}}) > -11.6$  (see Fig. 1). This box is drawn in a subjective way to include most of the known hard-TeV objects and to obtain a sizeable but still manageable number of candidates. Within this box, the probability of finding extreme TeV-peaked BL Lacs should increase to  $\gtrsim 60\%$ , according to the ratio of Hard-TeV vs Soft-TeV sources detected so far.

However, a gamma-ray peak at multi-TeV energies is not the only reason for a BL Lac to have a large  $\alpha_{x\gamma}$ . Regular HBL can

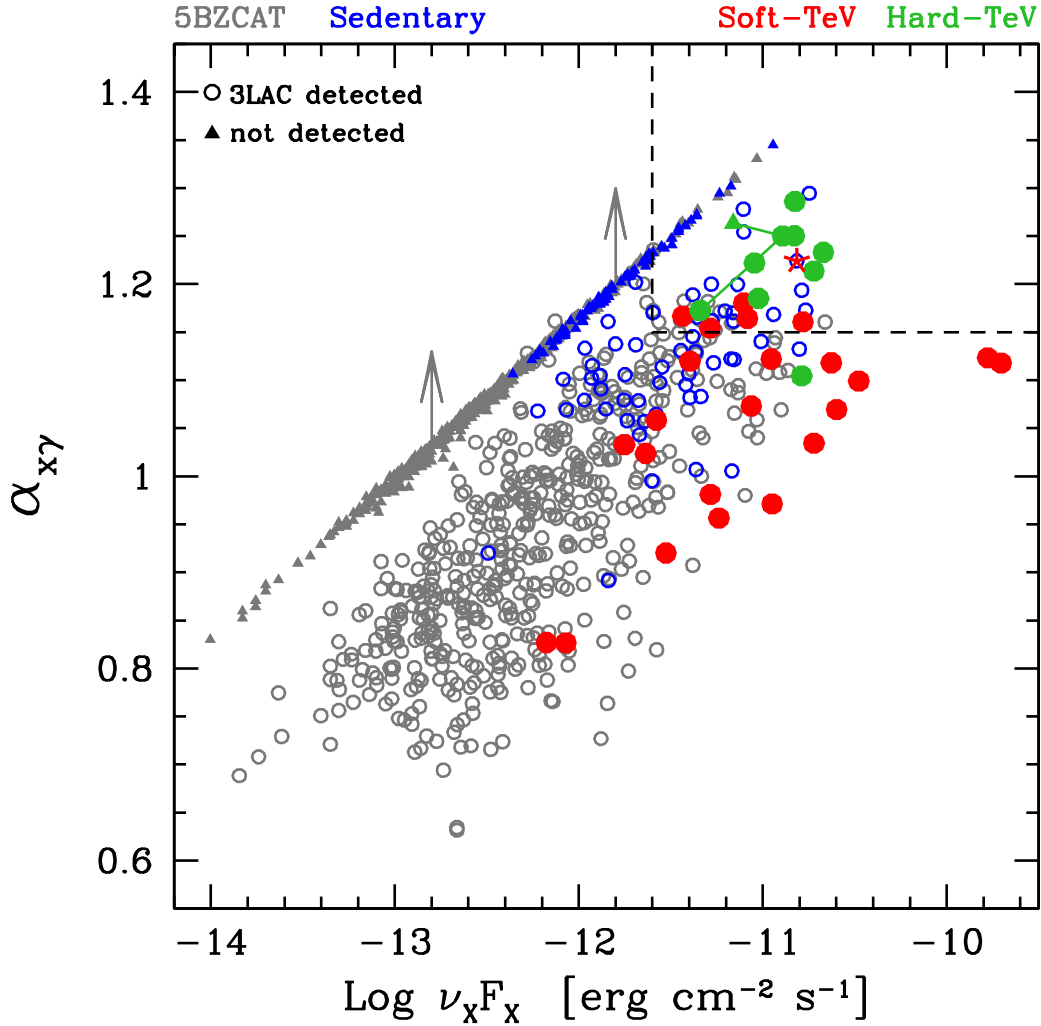


**Figure 1.** Plane of the broad-band index  $\alpha_{x\gamma}$  vs the X-ray  $\nu F_\nu$  flux at 1 KeV, for all BL Lacs in the Sedentary Survey and 5BZCAT samples (blue and grey markers, respectively). Gamma-ray data are obtained from the Fermi 3LAC catalog (open circles). For non-detected objects (triangles), a reference flux of  $8e-11 \text{ cm}^{-2} \text{ s}^{-1}$  (in the 1-100 GeV band) is adopted as upper limit (see text). This translates to a lower limit to  $\alpha_{x\gamma}$ , as indicated by the arrows. Given the correlation between the axes, the non-detected objects form a line in the figure (whose scatter is given by the K-correction). Hard-TeV BL Lacs (green full circles) cluster in the upper quadrant, while soft-TeV BL Lacs (red full circles) show lower  $\alpha_{x\gamma}$  values. The red star marks the position of 1ES 1426+428, which is extreme in synchrotron but not in TeV. The green lines connect the positions of the prototypical hard-TeV BL Lac 1ES 0229+200 in 3 different states (Costamante et al. in preparation): 1) during the first 2 years of *Fermi* operation (upper limit from the 2LAC catalog with same-epoch Swift data); 2) detection in years 2011-2013 with average RXTE flux in the same epoch; 3) 3LAC catalog values as the other objects.

still be found inside the selection box simply because of a lower Compton dominance, due to – for example – higher magnetic fields in the emitting region. In fact, considering a simple one-zone SSC scenario, higher synchrotron peak frequencies would tend to reduce the Compton dominance, all else being equal, due to the decrease of seed photons available for Thomson scattering (see for example Fig. 2 in Costamante & Ghisellini 2002).

In order to further reduce the chance of spurious objects, two additional cuts are introduced. The first is based on the gamma-ray spectral slope, if the object is detected in the 3LAC or in the Third Catalog of Hard Fermi LAT Sources (3FHL, Ajello et al. 2017): namely, if the photon index  $\Gamma_{3\text{LAC}} > 2.2$  or  $\Gamma_{3\text{FHL}} > 2.4$ . These values are larger than the typical  $1\sigma$  error in these data, indicat-

ing that the source has most likely a steep GeV spectrum locating the gamma-ray peak below 1 and 10 GeV, respectively. This cut excludes 6 objects.

The second cut is based on the broad-band colour-colour diagram with the WISE infrared flux, plotted in Fig. 2. The W3 filter is chosen as best compromise between infrared sensitivity and the minimization of the contribution of the host galaxy (see e.g. Fig. 2 in Arsioli et al. 2015). The hard-TeV objects tend again to cluster towards *low values* of  $\alpha_{\text{wx}}$ , indicating that they have a harder slope between infrared and X-ray energies than regular HBL. This is to be expected when the synchrotron emission peaks in the X-ray band, and the W3 flux is dominated by the non-thermal emission from the jet. Nonetheless, the W3 band can still be contaminated by

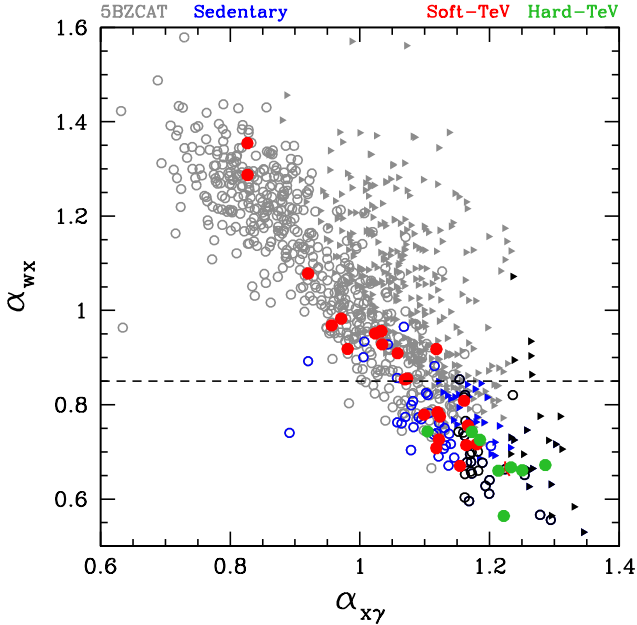


**Figure 2.** Colour-colour diagram of the broad-band spectral index  $\alpha_{\text{wx}}$  (between WISE W3 and 1 keV energies) vs  $\alpha_{\text{x}\gamma}$  (between 1 KeV and 1 GeV). Labels and markers as in Fig. 1. Triangles represents lower limits to  $\alpha_{\text{x}\gamma}$  for the objects not detected in the 3LAC. The dashed line shows the cut at  $\alpha_{\text{wx}} < 0.85$ . Black markers correspond to the objects inside the box in Fig. 1.

the host galaxy depending on the ratio between thermal and non-thermal emission in each object (Arsioli et al. 2015; Chang et al. 2017). Since this contamination can keep  $\alpha_{\text{wx}}$  higher than it should, the cut is applied rather loosely at  $\alpha_{\text{wx}} < 0.85$  (see Fig. 2). This cut reduces the number of candidates by a further 7 objects. None of these is detected in the 3LAC, while only two are marginally detected in the 3FHL with hints of steep spectrum, as expected.

The final list of 47 best candidates for a hard TeV emission is reported in Table 1, sorted according to their X-ray  $\nu F_{\nu}$  flux and excluding those objects with published VHE spectrum.

## 5 COMPARISON WITH PREVIOUS SELECTIONS

Most criteria proposed so far for TeV observations are developed to maximize the chance of detection, thus aiming at high VHE fluxes. These criteria are less suited for finding hard-TeV objects, and in fact might be biased *against* them.

Selections based on the *Fermi*-LAT detection or spectrum (e.g. Tavecchio et al. 2010) are not very effective since all HBL tend to have hard LAT spectra, and a high *Fermi*-LAT flux is more indicative of TeV softness rather than hardness, as shown before. Selections based on SSC modeling are generally flawed by construction, because the set of parameters and physical conditions valid for most HBL are not able to reproduce the hard TeV spectra. The shape of the SED in the synchrotron hump is very similar between normal and TeV-peaked HBL. Without knowing a-priori that the source is TeV-peaked, the resulting TeV spectra are regularly steep, especially when fitting the whole synchrotron hump from IR frequencies upwards (see e.g. Costamante et al. 2018). This type of

SSC modeling provides therefore good predicting power only for soft-TeV HBL.

The curvature of the X-ray spectrum (Massaro et al. 2011) does not seem a discriminating feature: hard-TeV BL Lacs show curvature values near the peak in the range 0.2–0.4 (Costamante et al. 2018), similar to soft-TeV HBL.

Selection schemes based on optical or IR colour diagrams alone, as the WISE blazar strip (Massaro et al. 2013), generally lose effectiveness for extreme BL Lacs (Chang et al. 2017). As the SED peaks shift at higher energies, the jet luminosity in the optical/infrared bands tends to become subdominant with respect to the thermal component of the host elliptical galaxy, both because of the peak shift and because of the overall lower luminosity, if the blazar sequence holds.

The selection by Bonnoli et al. (2015) is based on a high X-ray to Radio flux ratio ( $F_{\text{x}}/F_{\text{r}} > 10^4$ ) –similar to the value used for the Sedentary Survey and in Costamante et al. (2001)– and an optical spectrum dominated by the host galaxy. The latter condition is achieved by using the list by Plotkin et al. (2011), which is also limited in redshift to  $z \leq 0.4$ . These criteria are effective to select extreme *synchrotron* BL Lacs, but do not provide any direct indication of the location of the gamma-ray peak. Of the 9 objects in Bonnoli et al. (2015), three are included in the present selection as well (see Table 1), namely RBS 0723, 1ES 0927+500 and RBS 0921. Two other objects are left out but by a small margin, and thus can be considered good candidates also according to our criterium. These are RBS 1510 (out for  $\alpha_{\text{x}\gamma} = 1.145$ ) and RBS 1029 (out for  $\log(F_{\text{x}}) = -11.63$ ).

Recently Foffano et al. (2019) proposed a new selection. It is focused again on extreme *synchrotron* BL Lacs from the Swift-BAT 105-months source catalog which are also detected by *Fermi*-LAT in the 3LAC catalog. The synchrotron peak position is estimated directly from archival Swift-XRT, Swift-BAT and BeppoSAX data. Their final sample of VHE targets have 8 objects in common with our total sample, 5 of which are included in our selection as well.

## 6 CONCLUSIONS

The finding of TeV-peaked BL Lacs clustering towards high values of  $\alpha_{\text{x}\gamma}$  and X-ray flux and low values of  $\alpha_{\text{wx}}$  provides a simple criterium to select new TeV-peaked candidates. The broad-band index  $\alpha_{\text{x}\gamma}$  is the most important parameter: the limit on the X-ray flux is introduced to increase the chance of detectability at VHE and to reduce spurious sources, but can be relaxed for observations with more sensitive telescopes.

No filter on redshift has been introduced at this stage of the selection. With the low EBL level close to galaxy counts confirmed by all recent analyses (e.g. Aharonian et al. 2006; Domínguez et al. 2011; Costamante 2013; Franceschini & Rodighiero 2017; Desai et al. 2019), detections at redshifts up to 1 and beyond are well possible even with the present generation of Cherenkov telescopes. However, with the observed fluxes and present telescopes, redshifts up to  $z \sim 0.2$ –0.25 seem to provide the best compromise between space volume (i.e. number of objects) and flux around 1 TeV, allowing for spectral measurements extended into the TeV range. This is optimal for identifying hard-TeV sources, since a spectrum over at least a decade in energy can better constrain the slope of a power-law fit, thanks to the longer arm. Furthermore, the EBL optical depth becomes less energy-dependent in the 1–8 TeV range, due to the shape of the EBL spectrum (Aharonian 2001; Costamante 2013). This improves the chance of detection at

the highest energies for intrinsically hard spectra. Nevertheless, a higher source activity or more sensitive instruments like the future Cherenkov Telescope Array (CTA, Acharya et al. 2013) can allow comparable results at larger distances.

No VHE flux estimates are given at this stage. Even with the *Fermi*-LAT data, there is no clear way yet to distinguish between a hard-TeV and soft-TeV SED without the VHE data. The typical SSC modeling is thus of no use for predicting TeV-peaked sources, since it tends to systematically underestimate both flux and hardness of the spectrum in the TeV range. Besides, in these objects SSC might not be the correct gamma-ray mechanism to begin with.

An important advantage of the  $\alpha_{x\gamma}$  criterium is to by-pass the radio information. It is thus useful to explore also the faint end of the radio luminosity function, where low-luminosity but still jetted AGN can be difficult to recognize in large radio and optical surveys. Indeed, if the blazar sequence holds, the most extreme blazars might even be hidden in the radio quiet AGN population, since the low radio flux from the jet might not be “loud” enough with respect to the optical flux of the giant elliptical host galaxy (Ghisellini 1999; Costamante et al. 2007).

Both types of extreme blazars (synchrotron and TeV) become brightest in the X-ray band. In this respect the results from the first all-sky survey in hard X-rays soon to be provided by eROSITA (Merloni et al. 2012) will be optimal to find such objects, in particular when coupled with the recently-released 8-years *Fermi*-LAT catalog (4FGL, The *Fermi*-LAT collaboration 2019), the deepest all-sky survey so far in gamma-rays. Still, TeV-peaked BL Lacs can be truly identified and studied only through VHE data. Observations in the last decade have shown that essentially all BL Lacs (in fact all blazars) can copiously emit VHE gamma-rays, under proper conditions. In this respect, the importance of an unbiased extra-galactic sky survey at VHE at  $\sim 1$ -2% Crab-level sensitivity –as finally possible with CTA– cannot be overstated, given also the new type of population studies (logN-logS, luminosity functions etc.) and discovery potential that it opens. Nonetheless, the present generation of Cherenkov telescopes retains a lot of potential for expanding and studying the population of TeV-peaked BL lacs. Several other objects might exist, similar to 1ES 0229+200 or 1ES 1101-232 in flux and features, which simply have not been pointed yet.

## ACKNOWLEDGEMENTS

This research has made use of archival data, software and on-line services provided by the ASI Space Science Data Center (SSDC), and of data products from the Wide-field Infrared Survey Explorer, which is a joint project of the University of California, Los Angeles, and the Jet Propulsion Laboratory/California Institute of Technology, funded by the National Aeronautics and Space Administration. This research has made use of the NASA/IPAC Extragalactic Database (NED), which is operated by the Jet Propulsion Laboratory, California Institute of Technology, under contract with the National Aeronautics and Space Administration. This research has made use of data and software provided by the High Energy Astrophysics Science Archive Research Center (HEASARC), which is a service of the Astrophysics Science Division at NASA/GSFC and the High Energy Astrophysics Division of the Smithsonian Astrophysical Observatory.

## REFERENCES

- Abdo A. A., et al., 2009, *ApJ*, 707, 1310  
 Abdo A. A., et al., 2010, *ApJ*, 716, 30  
 Abeyssekara A. U., et al., 2016, *MNRAS*, 459, 2550  
 Abramowski A., et al., 2010, *A&A*, 516, A56  
 Abramowski A., et al., 2012, *A&A*, 538, A103  
 Acciari V. A., et al., 2009, *ApJ*, 695, 1370  
 Acciari V. A., et al., 2010, *ApJ*, 715, L49  
 Acharya B. S., et al., 2013, *Astroparticle Physics*, 43, 3  
 Ackermann M., et al., 2015, *ApJ*, 810, 14  
 Aharonian F. A., 2001, International Cosmic Ray Conference, 27, 250  
 Aharonian F. A., 2004, Very high energy cosmic gamma radiation : a crucial window on the extreme Universe. World Scientific, doi:10.1142/4657  
 Aharonian F. A., et al., 1999, *A&A*, 349, 11  
 Aharonian F., et al., 2006, *Nature*, 440, 1018  
 Aharonian F., et al., 2007a, *A&A*, 470, 475  
 Aharonian F., et al., 2007b, *A&A*, 473, L25  
 Aharonian F., et al., 2007c, *A&A*, 475, L9  
 Aharonian F., Buckley J., Kifune T., Sinnis G., 2008a, *Reports on Progress in Physics*, 71, 096901  
 Aharonian F. A., Khangulyan D., Costamante L., 2008b, *MNRAS*, 387, 1206  
 Aharonian F., et al., 2010, *A&A*, 521, A69  
 Ahnen M. L., et al., 2017, *MNRAS*, 468, 1534  
 Ahnen M. L., et al., 2018, *A&A*, 620, A181  
 Ajello M., et al., 2017, *ApJS*, 232, 18  
 Aleksić J., et al., 2014, *A&A*, 563, A90  
 Aliu E., et al., 2014, *ApJ*, 782, 13  
 Archambault S., et al., 2015, *ApJ*, 808, 110  
 Arsioli B., Fraga B., Giommi P., Padovani P., Marrese P. M., 2015, *A&A*, 579, A34  
 Arsioli B., Barres de Almeida U., Prandini E., Fraga B., Foffano L., 2018, *MNRAS*, 480, 2165  
 Atwood W. B., et al., 2009, *ApJ*, 697, 1071  
 Bonnoli G., Tavecchio F., Ghisellini G., Sbarrato T., 2015, *MNRAS*, 451, 611  
 Böttcher M., Dermer C. D., Finke J. D., 2008, *ApJ*, 679, L9  
 Chang Y.-L., Arsioli B., Giommi P., Padovani P., 2017, *A&A*, 598, A17  
 Costamante L., 2012, preprint, (arXiv:1208.0808)  
 Costamante L., 2013, *International Journal of Modern Physics D*, 22, 1330025  
 Costamante L., Ghisellini G., 2002, *A&A*, 384, 56  
 Costamante L., et al., 2001, *A&A*, 371, 512  
 Costamante L., Aharonian F., Khangulyan D., 2007, in Ritz S., Michelson P., Meegan C. A., eds, American Institute of Physics Conference Series Vol. 921, The First GLAST Symposium. pp 157–159, doi:10.1063/1.2757291  
 Costamante L., Bonnoli G., Tavecchio F., Ghisellini G., Tagliaferri G., Khangulyan D., 2018, *MNRAS*, 477, 4257  
 Desai A., Helgason K., Ajello M., Paliya V., Domínguez A., Finke J., Hartmann D., 2019, *ApJ*, 874, L7  
 Dolag K., Kachelrieß M., Ostapchenko S., Tomàs R., 2009, *ApJ*, 703, 1078  
 Domínguez A., et al., 2011, *MNRAS*, 410, 2556  
 Essey W., Kalashev O., Kusenko A., Beacom J. F., 2011, *ApJ*, 731, 51  
 Finke J. D., 2013, *ApJ*, 763, 134  
 Finke J. D., Reyes L. C., Georganopoulos M., Reynolds K., Ajello M., Fegan S. J., McCann K., 2015, *ApJ*, 814, 20  
 Foffano L., Prandini E., Franceschini A., Paiano S., 2019, *MNRAS*, 486, 1741  
 Fossati G., Maraschi L., Celotti A., Comastri A., Ghisellini G., 1998, *MNRAS*, 299, 433  
 Franceschini A., Rodighiero G., 2017, *A&A*, 603, A34  
 Ghisellini G., 1999, *Astrophysical Letters and Communications*, 39, 17  
 Ghisellini G., Righi C., Costamante L., Tavecchio F., 2017, *MNRAS*, 469, 255  
 Giommi P., Piranomonte S., Perri M., Padovani P., 2005, *A&A*, 434, 385

- Giommi P., Padovani P., Polenta G., Turriziani S., D'Elia V., Piranomonte S., 2012, *MNRAS*, **420**, 2899
- Hauser M. G., Dwek E., 2001, *ARA&A*, **39**, 249
- Jarrett T. H., et al., 2011, *ApJ*, **735**, 112
- Kalberla P. M. W., Burton W. B., Hartmann D., Arnal E. M., Bajaja E., Morras R., Pöppel W. G. L., 2005, *A&A*, **440**, 775
- Madhavan A. S. f., 2013, preprint, ([arXiv:1307.7051](https://arxiv.org/abs/1307.7051))
- Massaro F., Paggi A., Elvis M., Cavaliere A., 2011, *ApJ*, **739**, 73
- Massaro F., Paggi A., Errando M., D'Abrusco R., Masetti N., Tosti G., Funk S., 2013, *ApJS*, **207**, 16
- Massaro E., Maselli A., Leto C., Marchegiani P., Perri M., Giommi P., Piranomonte S., 2015, *Ap&SS*, **357**, 75
- Merloni A., et al., 2012, preprint, ([arXiv:1209.3114](https://arxiv.org/abs/1209.3114))
- Neronov A., Vovk I., 2010, *Science*, **328**, 73
- Padovani P., Giommi P., 1995, *ApJ*, **444**, 567
- Padovani P., Resconi E., Giommi P., Arsioli B., Chang Y. L., 2016, *MNRAS*, **457**, 3582
- Plotkin R. M., Markoff S., Trager S. C., Anderson S. F., 2011, *MNRAS*, **413**, 805
- Prosekin A., Essey W., Kusenko A., Aharonian F., 2012, *ApJ*, **757**, 183
- Resconi E., Coenders S., Padovani P., Giommi P., Caccianiga L., 2017, *MNRAS*, **468**, 597
- Stoeckel J. T., Morris S. L., Gioia I. M., Maccacaro T., Schild R., Wolter A., Fleming T. A., Henry J. P., 1991, *ApJS*, **76**, 813
- Tavecchio F., Ghisellini G., Ghirlanda G., Foschini L., Maraschi L., 2010, *MNRAS*, **401**, 1570
- Tavecchio F., Ghisellini G., Bonnoli G., Foschini L., 2011, *MNRAS*, **414**, 3566
- The Fermi-LAT collaboration 2019, preprint, ([arXiv:1902.10045](https://arxiv.org/abs/1902.10045))

This paper has been typeset from a  $\text{\TeX}/\text{\LaTeX}$  file prepared by the author.

**Table 2.** TeV-peaked BLLac candidates, sorted according to the X-ray flux considered as a tracer for their VHE flux.  $F_X$  is the RASS integral flux in the 0.1–2.4 keV band, as listed in the catalogs.  $\nu_\gamma F_\gamma$  and  $\nu_X F_X$  are the derived monochromatic  $\nu F_\nu$  fluxes at the respective energies. The broad-band indices  $\alpha_{x\gamma}$  and  $\alpha_{wx}$  are calculated from the Wise (W3 filter), X-ray (1 keV) and gamma-ray (1 GeV) monochromatic fluxes, including the K-correction. The  $\alpha_{rx}$  index is copied from the 5BZCAT. *Fermi*-LAT detection significances ( $\sigma$ ) in the 3FHL and 3LAC catalogs are also reported, together with the power-law photon index ( $\Gamma$ ) from the 3LAC catalog. In the last column, positive values mark objects in the Sedentary Survey sample (2 if also the redshift is taken from the Sedentary sample because absent in the 5BZCAT).

Name 5BZCAT	Source Name	$z$	$F_{[0.1-2.4 \text{ keV}]}$ $\text{erg cm}^{-2} \text{s}^{-1}$	$\nu_\gamma F_\gamma$ (1 GeV) $\text{erg cm}^{-2} \text{s}^{-1}$	$\nu_X F_X$ (1 keV) $\text{erg cm}^{-2} \text{s}^{-1}$	$\alpha_{x\gamma}$	$\alpha_{rx}$	$\alpha_{wx}$	$\sigma_{3\text{FHL}}$	$\sigma_{3\text{LAC}}$	$\Gamma_{3\text{LAC}}$	Sedent. (a)
5BZBJ0123+3420	1ES 0120+340	0.272	6.14e-11	2.64e-13	1.79e-11	1.294	0.490	0.556	8.9	9.6	1.48	1
5BZBJ0325-1646	RBS 0421	0.291	5.87e-11	1.45e-12	1.71e-11	1.173	0.460	0.654	16.3	18.9	1.79	1
5BZBJ1031+5053	1ES 1028+511	0.361	5.58e-11	9.94e-13	1.63e-11	1.194	0.480	0.628	18.8	18.9	1.71	1
5BZBJ0441+1504	SHBL J044127.4+150456	0.109	3.93e-11	9.34e-14	1.15e-11	1.345	0.450	0.529	-	-	-	2
5BZBJ0227+0202	RBS 0319	0.457	3.93e-11	1.10e-12	1.15e-11	1.168	0.500	0.596	6.9	11.1	2.04	1
5BZGJ0643+4214	B3 0639+423	0.089	3.18e-11	9.34e-14	9.28e-12	1.330	0.580	0.584	-	-	-	0
5BZBJ0509-0400	1ES 0507-040	0.304	2.70e-11	2.09e-13	7.88e-12	1.254	0.560	0.651	-	4.1	1.65	1
5BZBJ1417+2543	RBS 1366	0.237	2.70e-11	6.56e-13	7.88e-12	1.181	0.570	0.717	10.1	6.5	2.16	1
5BZBJ0930+4950	1ES 0927+500	0.187	2.69e-11	1.51e-13	7.85e-12	1.278	0.490	0.566	6.7	5.1	1.45	1
5BZBJ1422+5801	1ES 1421+582	0.635	2.50e-11	4.45e-13	7.29e-12	1.200	0.470	0.611	7.8	7.0	2.02	1
5BZGJ1504-0248	QUEST J1504-0248	0.217	2.46e-11	9.34e-14	7.18e-12	1.309	0.546	0.775	-	-	-	0
5BZGJ0425-0833	EXO 0423.4-0840	0.039	2.40e-11	9.34e-14	7.00e-12	1.311	0.614	0.706	-	-	-	0
5BZBJ1136+6737	RX J1136.5+6737 <sup>a</sup>	0.136	2.38e-11	7.11e-13	6.94e-12	1.161	0.540	0.734	14.5	15.3	1.72	1
5BZBJ0847+1133	RBS 0723 <sup>a</sup>	0.198	2.38e-11	6.21e-13	6.94e-12	1.170	0.520	0.695	11.6	10.5	1.74	1
5BZGJ2042+2426	RGB J2042.1+2426	0.104	2.32e-11	7.32e-13	6.77e-12	1.159	0.614	0.741	8.1	8.4	1.87	0
5BZBJ0314+0619	RBS 0400	-	2.29e-11	9.34e-14	6.68e-12	1.301	0.520	0.717	5.9	-	-	1
5BZBJ1456+5048	RBS 1444	0.479	2.21e-11	9.34e-14	6.45e-12	1.295	0.422	0.565	-	-	-	0
5BZBJ2357-1718	RBS 2066	-	2.14e-11	5.35e-13	6.24e-12	1.172	0.550	-	7.0	8.6	1.80	1
5BZBJ0837+1458	87GB 083437.4+150850	0.278	1.95e-11	9.34e-14	5.70e-12	1.291	0.572	0.724	-	-	-	0
5BZBJ0506-5435	RBS 621	-	1.69e-11	6.13e-13	5.51e-12	1.152	0.556	0.743	15.2	14.9	1.60	0
5BZBJ1535+5320	1ES 1533+535	0.89	1.79e-11	3.03e-13	5.22e-12	1.200	0.510	0.641	-	4.1	1.96	2
5BZBJ0244-5819	RBS 351	0.265	1.57e-11	4.39e-13	4.58e-12	1.163	0.631	0.765	11.1	10.4	1.70	0
5BZGJ1804+0042	RGB J1804+007	0.07	1.52e-11	9.34e-14	4.44e-12	1.277	0.695	0.776	-	-	-	0
5BZBJ0110-1255	RBS 161	0.234	1.51e-11	4.34e-13	4.41e-12	1.165	0.510	0.678	-	5.8	1.93	1
5BZBJ2343+3439	SHBL J234333.8+344004	0.366	1.51e-11	3.70e-13	4.41e-12	1.171	0.550	0.679	8.9	6.8	1.75	1
5BZGJ1056+0252	RBS 0921	0.236	1.49e-11	9.34e-14	4.35e-12	1.272	0.440	-	-	-	-	1
5BZBJ1516-1523	RXSJ15163-1523	-	1.46e-11	9.34e-14	4.26e-12	1.269	0.470	-	-	-	-	1
5BZBJ0018+2947	RBS 0042	0.1	1.43e-11	3.00e-13	4.17e-12	1.189	0.550	0.677	7.9	5.0	1.86	1
5BZBJ0216+2314	RBS 0298	0.288	1.40e-11	9.34e-14	4.08e-12	1.266	0.560	0.665	6.1	-	-	1
5BZBJ2138-2053	RBS 1769	0.29	1.33e-11	9.34e-14	3.88e-12	1.262	0.500	0.658	-	-	-	1
5BZBJ0503-1115	SHBL J050335.3-111507	-	1.29e-11	9.34e-14	3.76e-12	1.260	0.490	0.627	-	-	-	1
5BZBJ1848+4245	RGB J1848+427	-	1.28e-11	2.67e-13	3.73e-12	1.183	0.574	0.660	6.4	6.3	1.66	0
5BZBJ0014-5022	RBS 0032	-	1.23e-11	3.66e-13	3.59e-12	1.162	0.523	0.604	-	5.7	1.92	0
5BZBJ0140-0758	RBS 0231	-	1.19e-11	9.34e-14	3.47e-12	1.254	0.550	0.664	-	-	-	1
5BZBJ1257+2412	1ES 1255+244	0.141	1.17e-11	9.34e-14	3.41e-12	1.257	0.520	0.667	-	-	-	1
5BZGJ0303+0554	RBS 0384	0.196	1.16e-11	9.34e-14	3.38e-12	1.255	0.560	0.750	-	-	-	1
5BZBJ1021+1625	BZB J1021+1625	-	1.15e-11	9.34e-14	3.37e-12	1.252	0.540	0.695	-	-	-	0
5BZBJ1008+4705	RXJ10081+4705	0.343	1.13e-11	9.34e-14	3.30e-12	1.249	0.460	-	-	-	-	1

<sup>a</sup> Announced detected at VHE, but not published yet.

Table 2 – continued

Name	Source Name	$z$	$F_{[0.1-2.4 \text{ keV}]}$ $\text{erg cm}^{-2} \text{s}^{-1}$	$\nu_{\gamma} F_{\gamma}$ (1 GeV) $\text{erg cm}^{-2} \text{s}^{-1}$	$\nu_{\text{X}} F_{\text{X}}$ (1 keV) $\text{erg cm}^{-2} \text{s}^{-1}$	$\alpha_{\text{x}\gamma}$	$\alpha_{\text{rx}}$	$\alpha_{\text{wx}}$	$\sigma_{3\text{FHL}}$	$\sigma_{3\text{LAC}}$	$\Gamma_{3\text{LAC}}$	Sedent. (a)
5BZBJ1008+4705	RXJ10081+4705	0.343	1.13e-11	9.34e-14	3.30e-12	1.249	0.460	-	-	-	-	1
5BZBJ2123-1036	BZBJ2123-1036	-	1.08e-11	9.34e-14	3.15e-12	1.247	0.688	-	-	-	-	0
5BZBJ1237+3020	RXJ12370+3020	0.7	1.06e-11	9.34e-14	3.09e-12	1.238	0.470	-	-	-	-	2
5BZBJ0422+1950	MS 0419.3+1943	0.516	9.98e-12	9.34e-14	2.91e-12	1.237	0.500	0.726	-	-	-	1
5BZBJ2249-1300	RXSJ22491-1300	-	9.73e-12	9.34e-14	2.84e-12	1.240	0.490	-	-	-	-	1
5BZBJ1319+1405	RGB J1319+140	0.573	9.33e-12	2.67e-13	2.72e-12	1.161	0.634	0.816	-	4.3	1.87	0
5BZBJ1536+0138	MS 1534.2+0148	0.311	8.82e-12	9.34e-14	2.57e-12	1.232	0.624	0.695	-	-	-	0
5BZBJ1636-1248	BZB J1636-1248	0.246	8.74e-12	9.34e-14	2.55e-12	1.233	0.570	0.730	-	-	-	1
5BZBJ1140+1528	BZB J1140+1528	0.244	8.73e-12	8.41e-14	2.55e-12	1.236	0.640	0.821	7.3	5.2	1.40	0
5BZBJ1757+7033	MS 1757.7+7034	0.407	8.68e-12	2.11e-13	2.53e-12	1.170	0.520	0.747	5.6	5.5	1.71	1

**APPENDIX A: DATA TABLES IN ARXIV VERSION**

This ArXiv version of the paper includes in the source files the following data, for better usability: the ascii-only versions of Table 2, Table 2 sorted by RA and an additional table obtained with no limit on the X-ray flux, but with a stricter cut of  $\alpha_{x\gamma} \geq 1.2$ , sorted by decreasing X-ray flux.